# Estimation of Thermochemical Properties of Propellants Using Peng-Robinson Equation of State

Luciana Amorim da Silva[1] (ID), Ana Carolina Marotti Dias[1] (ID), Hector Gabriel Teixeira Volskis[2] (ID), José Daniel Langendorf da Silva[1] (ID), Aline Cardoso Anastacio[1] (ID), Fernando Cunha Peixoto[1,*] (ID)

1. Instituto Militar de Engenharia ROR – Departamento de Ensino e Pesquisa – Seção de Engenharia Química – Rio de Janeiro/RJ – Brazil. 2. Instituto Militar de Engenharia ROR – Departamento de Ensino e Pesquisa – Seção de Engenharia Mecânica – Rio de Janeiro/RJ – Brazil.

*Correspondence author: fpeixoto@ime.eb.br

## ABSTRACT

Several aspects make nitrocellulose based powders adequate as a solid propellant for rockets and missiles and the prefe rable propellant to be used in firearms and artillery: it produces less smoke and less fouling than other propellants; its burning rate shows a well-defined relation to pressure and the composition of the gaseous mixture resulting from its decomposition by burning can be predicted with relatively high levels of accuracy. This last feature, if coupled with adequate thermodynamic models, leads to a reliable framework for the simulation of internal ballistics and, ultimately, to an efficient design. Some simpler models use an ideal gas approach, which is obviously not adequate, and some others perform corrections based on the Virial E quation of S tate for sake of algebraic simplicity. This work employs the Peng-Robinson equation of state to model the pressure-volume-temperature (PVT) behavior of the gases produced during the burning reaction, once it is known to be accurate in the high pressures obtained inside combustion chambers. The results were compared to experimental data obtained in a closed vessel device and showed that the Peng-Robinson equation of state could predict the chamber pressure with higher accuracy.

Keywords: Internal ballistics; Barreled guns; Ballistic cycle.

## INTRODUCTION

Propellants are a class of explosives that, when properly initiated, can burn in a rapid and controlled manner, a process termed deflagration, thus generating enough gaseous products to propel a weapon projectile (Venugopalan 2015). Despite the drawbacks of producing a large volume of soot and smoke during its combustion, black powder was the first gun propellant ever made, being used for hundreds of years. From the nineteenth century on, this scenario came to be profoundly modified with the discovery of nitrocellulose (NC). This newfound substance became the main ingredient of propellants, resulting in an improved performance, with practically no combustion residue. Due to this feature, these propellants came to be called smokeless powder. Even though they are called powders, they are designed as grains that display different geometric shapes,

such as: flakes, ribbons, spheres, cylinders or tubes. Every shape will present a specific burn area which will affect the burn ratio. Along with a lot of possibilities regarding grain shape and size, the smokeless propellants also vary conforming to the ingredients selected.

Conventional propellants are classified according to its composition, mainly the energetic base. When there is only NC as the energetic base, the propellant is called a single-base (SB) type. It can be employed in several systems, from handguns, as pistols and revolvers, to artillery weapons, rockets and missiles. When the propellant is made of NC and nitroglycerine (NG) as the energetic base, it is said to be double-base (DB) type. The presence of a second ingredient makes them more energetic, however a proper care regarding the percentage of NG must be taken, since too much energy makes the gases hotter than necessary, causing erosion to nozzles and barrels, thus reducing its service life. DB applications involve some pistol ammunition, but mostly mortar augmenting charges and military rockets and missiles. Triple-base (TB) propellants receive this classification for being made of NC, NG and nitroguanidine (NGu). NGu is a component whose main contribution is to decrease the adiabatic flame temperature; thus, a TB propellant is applied for large caliber naval guns and artillery weapons with a high rate of fire. Lastly, there is the multibase or nitramine propellant, which is an evolution of the triple base, where NGu is partly or completely replaced by RDX (cyclotrimethylenetrinitroamine). In terms of energy, a nitramine propellant remains between TB and DB.

When developing new propellants formulations or designing new improved-performance systems, a main concern must be a more accurate and more reliable estimation of thermochemical parameters, such as projectile muzzle velocity and chamber pressure. Usually, the only input available for the calculation of these parameters are the loading density and the propellant's composition. Therefore, obtaining precise data to implement into internal ballistics' models is a major concern. In order to address this problem, one should take into account mechanical, kinetic, geometric and combustion thermodynamics aspects (Suceska, 1999; H. M. Stationary Office, 1987; Harvazinski and Talley, 2018; Dyer *et al.*, 2007); Congiunti and Bruno, 2003; Hickey and Ihme , 2013)

In this paper, a case study of a propellant combustion under closed volume conditions is presented to determine thermodynamic factors that affect internal ballistic. These factors comprehend the composition of combustion products assuming water-gas equilibrium and the calculation of energy balance, adiabatic flame temperature and chamber pressure. Moreover, a special highlight to the difficulties involving the selection of a proper mathematical model to describe the chemical equilibrium in combustion products must be considered. Many studies approaching this problem have chosen the classical Virial-2 equation of state (EoS) to represent real gases (Saurel and Neron, 2021; Suceska, 1999; Xu *et. al.*, 2016) and, to our best knowledge, this choice is based only on the algebraic convenience (Longdon 1987). However, the classical Virial-2 equation of state presents relevant deviations when modeling high pressures and temperatures phenomena, due to its quadratic form (Prausnitz *et al.* 2000). To tackle these limitations, a Peng-Robinson Equation of State (PR-EoS), which has a cubic form, is selected, because of its known reliability when modeling high pressure gaseous systems (Bergan 1991; Congiunti and Bruno 2003; Giorgi *et al.* 2014; Hickey and Ihme 2013; Jofre and Urzay 2021; Mallepally *et al.* 2019; Müller *et al.* 2017; Müller and Pfitzner 2017; Myint *et al.* 2016). Additionally, we report the results of a case study where computer simulations were conducted to predict the combustion chamber pressure using the PR-EoS for a DB propellant formulation. These computer results using PR-EoS were compared to the classical Virial-2 EoS approach and to experimental data obtained from a (ballistic) closed vessel.

## METHODOLOGY

### Experimental Protocol

Even though parameters such as chamber pressure and others are necessary for the design of guns and propellant charges, a gun barrel is not a suitable apparatus for determining transient high pressures and how they change over time due to the rapid

forward movement of the projectile, the gas and the burning propellant. For measuring transient pressures, a constant volume condition is mandatory, and the suitable apparatus for that is the closed vessel (Grivell 1982; Mukhtar *et al.* 2019).

A Closed Vessel Test consisted on enclosing and burning a propellant charge of formulation A within a vessel of constant volume to estimate their ballistic parameters (Oliveira *et al.* 2005). The equipment is represented in Fig. 1:



Source: Elaborated by the authors.

**Figure 1.** Closed Vessel.

This test was conducted for six different loading densities (Mehta *et al.* 2015). After closing the vessel, the charge was ignited by the passage of electric current through a filament that dazzled and ignited a small amount of priming (black powder). Although black powder was used, it is also very common to use squibs for this purpose. This ignition was remotely controlled by a computer that acquired pressure versus time data. The closed vessel has a chamber volume of 200 cm$^3$ and the tested charges had loading densities of 0.1, 0.12, 0.14, 0.16, 0.18 and 0.20 g/cm$^3$. The charge dimensions were 17.5 cm x 15.3 cm x 0.038 cm and the composition of Formulation A is described in Table 1.

**Table 1.** Chemical composition of propellant formulation A.

| Formulation A | Composition |
|---|---|
| NC (12.5% N) | 57.65% |
| NG | 39.4% |
| Resorcinol | 1% |
| Centralite I | 1.95 |

Source: Elaborated by the authors.

Before plotting the pressure versus time data, the equipment manufacturer was contacted to provide the storage structure of the data in the output (binary) file. The encoding provided is shown in Table 2.

With the format provided, a program was built for the decoding of this information and its availability for later statistical treatment was stored in a vector variable termed as $P^{exp}$, with a component for each of the 3072 time points acquired.

**Table 2.** Data structure in PE7 files.

| Description | Initial Position on Binary File | Type/Size |
|---|---|---|
| Powder Type | 0 | 1 byte |
| Propellant | 1 | 13 char. string |
| Batch | 14 | 13 char. string |
| Manufacture Date | 27 | 11 char. string |
| Receiving Date | 38 | 11 char. string |
| Testing Date | 49 | 11 char. string |
| Operator | 60 | 13 char. string |
| Vessel ID | 73 | 13 char. string |
| Transductor | 86 | 13 char. string |
| Serial Number | 99 | 13 char. string |
| Sensitivity | 112 | 8 digits real |
| Volume | 120 | 8 digits real |
| Propellant Mass | 128 | 8 digits real |
| Gain | 136 | 8 digits real |
| Sampling Interval | 144 | 8 digits real |
| Temperature | 152 | 8 digits real |
| Shot Delay | 160 | 8 digits real |
| Pressure Unit | 168 | 1 byte |
| Series Number | 169 | 2 digits integer |
| Shot Number | 171 | 2 digits integer |
| Value 1 | 173 | 2 digits integer |
| Value 2 | 175 | 2 digits integer |
| … | … | … |
| Value 3071 | 6313 | 2 digits integer |
| Value 3072 | 6315 | 2 digits integer |

Source: Elaborated by the authors.

## Propellant formulation

The propellant deflagration is traditionally modeled as a decomposition reaction (Cooper and Kurowski 1997; Longdon 1987), which will be described as follows. The main component of DB propellants is NC (Longdon 1987), which can be obtained by the nitration of cellulose as described in Fig. 2.

As it can be seen, the monomer formula can be expressed as $C_6H_7O_2(OH)_{3-x}(ONO_2)_x$, where x can assume values from 1 to 3, which leads to a nitrogen content from 6.76% to 14.14%. Nitrocellulose can be gelatinized by an ether-alcohol mixture, acetone and even NG to generate a material that can be conformed into different shapes. Several substances are also incorporated, such as stabilizers (diphenylamine, ethyl centralite), plasticizers (dibutyl phthalate), flame suppressors (potassium salts) and burn rate modifiers (lead and copper salts), or added to the propellant surface to provide characteristics such as the ability to dissipate static electricity or to act as a solid lubricant (graphite) (Cooper and Kurowski 1997).
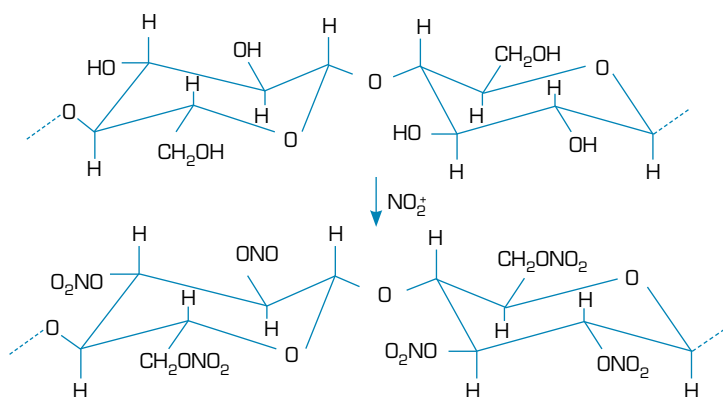
Source: Elaborated by the authors.

**Figure 2.** Cellulose nitration.

In general, the substances used on propellants only exhibit carbon, oxygen, hydrogen and nitrogen in their molecules, as can be seen on Table 3 (Rumble 2021).

**Table 3.** Moles of atoms in 1 gram of substance.

| Substance | Formula | C | H | N | O |
|---|---|---|---|---|---|
| NC | $C_6H_7O_2(OH)_{3-x}(ONO_2)_x$ | $6/162+45x$ | $10 - x / 162 + 45x$ | $x / 162 + 45 x$ | $5 + 2x / 162 + 45x$ |
| NG | $C_3H_5N_3O_9$ | 0.013210 | 0.022017 | 0.013210 | 0.039631 |
| DGDN | $C_4H_8N_2O_7$ | 0.020396 | 0.040791 | 0.010198 | 0.035692 |
| Nitroglicol | $C_2H_4N_2O_6$ | 0.013152 | 0.026304 | 0.013152 | 0.039456 |
| NGu | $CH_4N_4O_2$ | 0.009609 | 0.038434 | 0.038434 | 0.019217 |
| RDX | $C_3H_6N_6O_6$ | 0.013507 | 0.027014 | 0.027014 | 0.027014 |
| HMX | $C_4H_8N_8O_8$ | 0.013507 | 0.027014 | 0.027014 | 0.027014 |
| Oxamide | $C_2H_4N_2O_2$ | 0.022710 | 0.045419 | 0.022710 | 0.022710 |
| Dinitrotoluene | $C_7H_6N_2O_4$ | 0.038433 | 0.032943 | 0.010981 | 0.021962 |
| Resorcinol | $C_6H_6O_2$ | 0.054545 | 0.054545 | 0 | 0.018181 |
| Diethyl phthalate | $C_{12}H_{14}O_4$ | 0.053998 | 0.062997 | 0 | 0.017999 |
| Dibut yl phthalate | $C_{16}H_{22}O_4$ | 0.057484 | 0.079041 | 0 | 0.014371 |
| Diamyl phthalate | $C_{18}H_{26}O_4$ | 0.058749 | 0.084860 | 0 | 0.013055 |
| Centralite I | $C_{17}H_{20}N_2O$ | 0.063351 | 0.074531 | 0.007453 | 0.003727 |
| Centralite II | $C_{15}H_{16}N_2O$ | 0.062424 | 0.066585 | 0.008323 | 0.004162 |
| Vaseline | $C_{18}H_{38}$ | 0.070731 | 0.149322 | 0 | 0 |
| Diphenylamine | $C_{12}H_{11}N$ | 0.070916 | 0.065006 | 0.005909 | 0 |
| Camphor | $C_{10}H_{16}O$ | 0.065691 | 0.105105 | 0 | 0.006569 |
| Graphite | C | 0.083264 | 0 | 0 | 0 |

Source: Adapted from Rumble (2021).

Therefore, it is a common practice to express the reaction mixture as a hypothetical substance, with a formula given by $C_aH_bN_cO_d$, which is obtained as a mass-average of its constituents.

## Assumptions

To establish a model for propellant formulation designs, the following assumptions are made (Sudarsan *et al.* 2016):

- Burning of propellant is a continuous process, self-sustained, smooth and layered;
- Propellant combustion undergoes breaking of chemical bonds described by elementary reactions in accordance with Kisliakowsky-Wilson (K-W) rules and its modified version; and
- Equilibrium constant of water-gas equilibrium is temperature dependent only.

## Mathematical model

The following model is developed in three steps:

- Step 1 presents the oxygen balance for the explosive species;
- Step 2 calculates energy balance and adiabatic flame temperature;
- Step 3 gives thermochemical properties of propellant assuming water gas equilibrium and PR-EoS approach; and
- Step 4 implements thermodynamics data into a computer simulation framework.

## Oxygen balance

If the total combustion is achieved, as represented by the chemical reaction (Eq. 1):

$$C_aH_bN_cO_d \rightarrow aCO_2 + \frac{b}{2}H_2O + \frac{c}{2}N_2 + \frac{d-2a-\frac{b}{2}}{2}O_2 \tag{1}$$
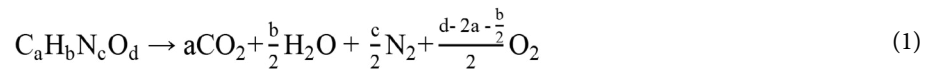
the oxygen balance ($\Omega$), which is the ratio between the remaining mass of oxygen and the original mass, is given by Eq. 2:

$$\Omega = \frac{d - 2a - b/2}{12a + b + 14c + 16d} 1600\% \tag{2}$$

It can be shown, from data on Table 3, that NC ($-73.4\% < \Omega < -24.2\%$) and NGu ($-30.7\%$) exhibit strongly negative values for $\Omega$ and only NG ($3.5\%$) exhibits a slightly positive one. In fact, for most propellants, $-50\% < \Omega < -30\%$, which leads to incomplete combustions, with the generation of $H_2$, CO and even C along with the gases shown in Eq. 1.

## Energy balance and the adiabatic flame temperature

The standard heat of combustion of propellants ($Qv$) is usually measured in an adiabatic calorimeter at constant volume, which leads to Eq. 3 (Van Ness *et al.* 2017):

$$Q_v = -\Delta U^0 = -\left[ \sum_p \Delta U_f^0 - \sum_r \Delta U_f^0 \right] \tag{3}$$

where $\sum_p \Delta U_f^o$ is the energy of formation of the gaseous products and $\sum_r \Delta U_f^o$ is the energy of formation of the reactants, both evaluated at standard conditions - usually 298 K - and given in Tables 4 and 5 (Longdon 1987).

**Table 4.** Energy of formation of reactants.

| Reactant | Molecular weight | $\Delta U_f^o$ (J/g) |
|---|---|---|
| NC | - | 260.564(%N) – 5790.308 |
| NG | 227.09 | -1602 |
| DGDN | 196.12 | -2197 |
| EGDN (Nitroglicol) | 152.06 | -1607 |
| NGu | 104.07 | -791 |
| RDX | 222.12 | +276 |
| HMX | 296.16 | +251 |

Continue…

**Table 4.** Continuation.

| Reactant | Molecular weight | $\Delta U_f^o$ (J/g) |
|---|---|---|
| Oxamide | 88.07 | -5657 |
| DNT (Dinitrotoluene) | 182.13 | -218 |
| Resorcinol | 110.11 | -3280 |
| DEP (Diethyl phthalate) | 222.23 | -3272 |
| DBP (Dibut yl phthalate) | 278.34 | -2929 |
| DAP (Diamyl phthalate) | 306.39 | -2845 |
| Centralite I | 268.35 | -481 |
| Centralite II | 240.29 | -510 |
| Vaseline | 254.48 | -1791 |
| DPA (Diphenylamine) | 169.23 | +937 |
| Graphite | 12.01 | 0 |

Source: Adapted from Longdon (1987).

**Table 5.** Energy of formation of (possible) products.

| Products | Molecular weight | $\Delta U_f^o$ (kJ/mol) |
|---|---|---|
| $CO_2$ | 44.01 | -393.5 |
| CO | 28.01 | -111.8 |
| $H_2O$ (l) | 18.02 | -282.0 |
| $H_2O$ (g) | 18.02 | -240.6 |
| ·OH | 17.01 | +41.4 |
| ·NO | 30.01 | +90.4 |
| ·H | 1.01 | +216.7 |
| ·N | 14.01 | +356.8 |
| ·O | 16.00 | +245.8 |
| $CH_4$ | 16.04 | -72.4 |
| $NH_3$ | 17.03 | -42.5 |
| $N_2$ | 28.01 | 0 |
| $H_2$ | 2.01 | 0 |

Source: Adapted from Longdon (1987).

Based on Table 4 and 5, it is possible to estimate the adiabatic flame temperature ($T_o$), which is the one achieved when the heat of combustion is used to heat the gaseous products, as in Fig. 3.
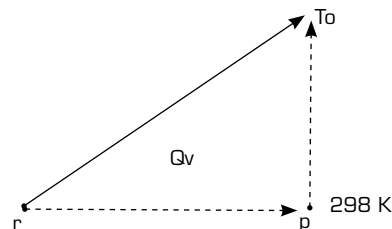


Source: Elaborated by the authors.

**Figure 3.** State-temperature diagram.

Assuming that the energy is not a function of pressure, it is straightforward to calculate $T_o$ (in K) (Eq. 4) based on the isochoric heat capacity ($C_v$) (in J/mol.k), which can be obtained by Eq. 5 (Van Ness $et\ al.$ 2017):

$$-\Delta U^o = \int_{298}^{To} C_v dT \tag{4}$$

$$C_v = C_p - R \tag{5}$$

where $R$ is the universal constant of gases and $C_p$ (in J/mol.K) is the isobaric heat capacity. This parameter can be calculated by applying a correlation for the gaseous products (Eq. 6) based only on the temperature (in K), where the required coefficients for each gas are given in Table 6 (Van Ness $et\ al.$ 2017).

$$C_p = C_1 + C_2 . T + C_3 . T^{-2} \tag{6}$$

**Table 6.** Parameters for the $C_p$ correlation.

| Product | C1 | C2 x 10³ | C3 x 10⁻⁵ |
|---|---|---|---|
| CO | 6.79 | 0.98 | -0.11 |
| $H_2O$ | 7.30 | 2.46 | 0 |
| $CO_2$ | 10.57 | 2.1 | -2.06 |
| $H_2$ | 6.52 | 0.78 | 0.12 |
| $N_2$ | 6.83 | 0.9 | -0.12 |

Source: Adapted from Van Ness $et\ al.$ (2017).

Considering that the energy balance and the adiabatic flame temperature depend on the composition of the gaseous mixture obtained, this topic will be addressed in the following section.

## Gaseous products and the water-gas equilibrium

It is assumed, at this point, that the combustion product is a mixture of CO, $CO_2$, $H_2$, $H_2O$ and $N_2$, with the first four being involved in the so-called water-gas equilibrium reaction (Eq. 7) (Rumble 2021):

$$CO(g) + H_2O(g) \leftrightarrow CO_2(g) + H_2(g) \tag{7}$$
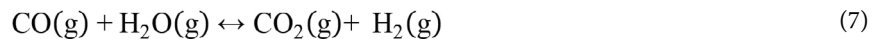
whose equilibrium constant is given by Eq. 8 (Smith $et\ al.$ 2010):

$$\ln(K) = \frac{-\Delta G^o}{R.T} = -\frac{\Delta H^o - T\Delta S^o}{R.T} = \frac{\Delta S^o}{R} - \frac{\Delta H^o}{R.T} = \frac{4577.8}{T} - 4.33 \tag{8}$$

where $\Delta G^o$ is the Gibbs free energy, $\Delta H^o$ is the enthalpy and $\Delta S^o$ is the entropy, all at standard condition.

Some works on ballistics relate this constant directly to the concentration of the gases involved ($CO_2$, $H_2$, CO and $H_2O$), assuming ideal gas behavior (Prausnitz $et\ al.$ 2000). Afterwards, a correction is conducted using the Virial equation of state (Van Ness $et\ al.$ 2017), truncated at its quadratic term (V-2 EoS) (Longdon 1987). The procedure built this way is somehow convenient, since it results in an iterative scheme for $T_o$, with the composition being calculated analytically in each iteration (Prausnitz $et\ al.$ 2000). Besides, it is algebraically independent of the pressure in the vessel, which is calculated after convergence is achieved (Longdon 1987).

In this work, we opted to use the Peng and Robinson Equation of State (PR-EoS) (Van Ness $et\ al.$ 2017), illustrated in Eq. 9, which shows to be more accurate for the high pressures found in ballistic cycles:

$$P = \frac{RT}{v-b} - \frac{a(T)}{v(v+b) + b(v-b)} \tag{9}$$

where $v$ is the molar volume, $R$ is the universal constant of gases, $T$ is the temperature and $a$ ($T$) and $b$ are parameters calculated by mixing rules given in Eqs. 10 and 11, as follows (Prausnitz *et al.* 2000):

$$a(T) = \sum_i \sum_j x_i x_j \sqrt{a_i(T) a_j(T)} \tag{10}$$

$$b = \sum_i x_i b_i \tag{11}$$

where $x_i$ is the molar fraction of "$i$". The parameters for individual species are related to their critical coordinates ($T_{c_i}$ and $P_{c_i}$) and their acentric factor ($\omega_i$) as follows in Eqs. 12 and 13 (Prausnitz *et al.* 2000):

$$a_i(T) = 0.45724 \frac{R^2 T_{c_i}^2}{P_{c_i}} \left[ 1 + (0.37464 + 1.54226\omega_i - 0.26992\omega_i^2)\left(1 - \sqrt{\frac{T}{T_{c_i}}}\right) \right]^2 \tag{12}$$

$$b_i = 0.0778 \frac{R \cdot T_{c_i}}{P_{c_i}} \tag{13}$$

The critical coordinates of gaseous species can be found in Table 7, along with their acentric factors (Prausnitz *et al.* 2000).

**Table 7.** Critical coordinates and acentric factors of the products.

| Product | Tc (K) | Pc (atm) | $\omega$ |
|---------|--------|----------|----------|
| CO | 132.85 | 34.48 | 0.045 |
| $H_2O$ | 647.14 | 217.75 | 0.344 |
| $CO_2$ | 304.12 | 72.78 | 0.225 |
| $H_2$ | 32.98 | 12.76 | -0.217 |
| $N_2$ | 126.20 | 33.54 | 0.037 |

Source: Retrieved from factors Prausnitz *et al.* (2000).

The equilibrium constant is related to the activities ($\hat{a}_i$) of the gases involved in the equilibrium, according to Eq. 14 (Van Ness *et al.* 2017):

$$K = \frac{\hat{a}_{CO_2} \hat{a}_{H_2}}{\hat{a}_{CO} \hat{a}_{H_2O}}, \text{ with } \hat{a}_i = \frac{\hat{f}_i}{f_i^o} = \frac{x_i \hat{\phi}_i P^o}{P^o} = x_i \hat{\phi}_i \tag{14}$$

where $\hat{f}_i$ is the fugacity of "$i$" in the mixture, $\hat{\phi}_i$ is the fugacity coefficient of "$i$" in the mixture and $f_i^o$ is the fugacity of "$i$" in the reference state, which can be considered the fugacity of the ideal gas in the same temperature, leading to $f_i^o = P^o$ for all components, thus leading to Eq. 15.

$$\ln K = \left[ \ln n_{CO_2} + \ln n_{H_2} - \ln n_{CO} - \ln n_{H_2O} \right] + \ln \hat{\phi}_{CO_2} + \ln \hat{\phi}_{H_2} - \ln \hat{\phi}_{CO} - \ln \hat{\phi}_{H_2O} \tag{15}$$

The fugacity coefficient can be calculated with Eq. 16 (Van Ness *et al.* 2017):

$$RT \ln \hat{\phi}_i = - \int_{\infty}^{V} \left[ \left( \frac{\partial P}{\partial n_i} \right)_{T,V,n_j} - \frac{RT}{V} \right] dV - R \ln Z \tag{16}$$

$$Z = \frac{PV}{nRT} \tag{17}$$

where $V$ is the volume, $R$ is the universal constant of gases, $T$ is the temperature and $Z$ is the compressibility factor, given by Eq. 17. Using Eqs. 9–11 in Eq. 16, one can find the fugacity coefficients for PR-EoS, based on Eqs. 18 and 19 (Van Ness *et al.* 2017).

$$\ln(\hat{\phi}_i) = \frac{b_i}{b}(Z - 1) - \ln(Z - B) - \frac{a}{2\sqrt{2}bRT}\left[\frac{2\sum_j a_{ij}x_j}{a} - \frac{b_i}{b}\right]\ln\left(\frac{Z+(1+\sqrt{2})B}{Z+(1-\sqrt{2})B}\right) \tag{18}$$

$$B = \frac{bP}{RT} \tag{19}$$

The reader must be aware that, even though $N_2$ is not involved in the equilibrium, it must be considered for the calculation of all fugacity coefficients.

Finally, the dependence of the energy to the molar volume (ultimately, to pressure itself) is incorporated, in order to correct Eq. 4. For that, the first law of thermodynamics is used, along with one of Maxwell relations (Van Ness *et al.* 2017), to give Eq. 20:

$$U - U^0 = \int_\infty^v \left[T\left(\frac{\partial P}{\partial T}\right)_v - P\right]dv \tag{20}$$

where $U^0$ is the energy of an ideal gas in the same conditions (emulated for $v \to \infty$), which is a function only of the temperature. From Eq. 9:

$$U - U^0 = \int_\infty^v \frac{\left[a(T) - \left(\frac{\partial a}{\partial T}\right)T\right]}{v(v+b)+b(v-b)}dv = \frac{\left[a(T) - \left(\frac{\partial a}{\partial T}\right)T\right]}{2b\sqrt{2}}\ln\left[\frac{v - (1-\sqrt{2})b}{v - (1+\sqrt{2})b}\right] \tag{21}$$

From equation 10:

$$\left(\frac{\partial a}{\partial T}\right) = \sum_i \sum_j \frac{x_i x_j}{2\sqrt{a_i a_j}}\left[a_j \frac{\partial a_i}{\partial T} + a_i \frac{\partial a_j}{\partial T}\right] \tag{22}$$

From equation 12:

$$\frac{\partial a_i}{\partial T} = \frac{a_i\left[-\left(0.37464 + 1.54226\omega_i - 0.26992\omega_i^2\right)(T.Tc_i)^{-1/2}\right]}{\left[1+\left(0.37464 + 1.54226\omega_i - 0.26992\omega_i^2\right)\left(1 - \sqrt{\frac{T}{Tc_i}}\right)\right]} \tag{23}$$

A detailed deduction of equations from Eqs. 18 to 23 can be found in the Appendix.

The complete framework is ready for numerical implementation at this point, but it is possible to reduce the number of variables (which is convenient for computational efficiency), by expressing the number of moles of each gaseous species in terms of the number of moles of $CO_2$, which can be achieved by an atom balance (Eq. 24).

$$\begin{cases} a = n_{CO_2} + n_{CO} \Rightarrow n_{CO} = a - n_{CO_2} \\ b = 2n_{H_2} + 2n_{H_2O} \Rightarrow n_{H_2O} = d - a - n_{CO_2} \\ d = 2n_{CO_2} + n_{CO} + n_{H_2O} \Rightarrow n_{H_2} = \frac{b}{2} - d + a + n_{CO_2} \\ c = 2n_{N_2} \Rightarrow n_{N_2} = \frac{c}{2} \end{cases} \tag{24}$$

## RESULTS AND DISCUSSION

When designing new propellants formulations, two important parameters must be investigated: the maximum pressure and the flame temperature. They can reflect the burning characteristics of propellants, because their performance parameters, such as burn rate, vivacity, force constant, co-volume and specific impulse are based on the knowledge of the chemical composition and these two parameters. Thus, the maximum pressure and the flame temperature are important input parameters in numerical simulations to predict performance properties. Therefore, looking into different approaches to improve accuracy in theoretical analysis is of great importance for developing new propellants formulations.

Therefore, this work used PR-EoS to estimate the maximum pressure of the propellant formulation A. The results were compared to the experimental values and the calculated value using classical Virial-2 EoS, in order to evaluate the accuracy of the PR-EoS in the calculations of this thermodynamic parameter.

## Calculation Results of Maximum Pressure

In order to explain why the pressure is important for propellants, it is worth briefly mentioning part of the ballistic cycle. When a propellant is ignited, within a few milliseconds, hot gases are produced from the burning surface of each grain, and the pressure in the chamber, that started to rise due to the ignition of the primer, keeps rising rapidly. Since most projectiles are resistant to propulsion, an extra force is required to separate the projectile from the case. This resistance makes the chamber pressure get even higher until it is sufficient to engrave the driving band. After that, the projectile starts to be released. Although the available volume increases as the projectile moves along the bore, since the burning rate is dependent on the chamber pressure, the rate of gas production is faster than the projectile speed inside the bore, so the pressure continues to increase up to its peak, until the projectile has moved some distance. After that, the pressure drops and by the time the projectile has reached the halfway point of the bore, the propellant is all-burned.

By knowing how this cycle works, it is possible to understand how the pressure dictates whether a shot will occur or not, whether the gases produced will be able to produce the desired thrust, leading to an expected muzzle velocity, and whether there will be damage to the barrel.

In this paper, we calculated the maximum pressure of formulation A under different loading densities. The calculated and reference values are shown in Table 8.

**Table 8.** Maximum pressure on the experiment and predicted chamber pressure as functions of the load density.

| $\Delta$ (g/cm³) | Experimental | V2-EoS | | PR-EoS | |
|---|---|---|---|---|---|
| | $P_{max}$ (MPa) | $P_{max}$ (MPa) | Deviation (%) | $P_{max}$ (MPa) | Deviation (%) |
| 0.10 | 121.6 | 110.3 | 9.3% | 126.4 | 3.9% |
| 0.12 | 151.6 | 134.4 | 11.3% | 154.5 | 1.9% |
| 0.14 | 174.6 | 159.2 | 8.8% | 183.9 | 5.3% |
| 0.16 | 214.4 | 184.7 | 13.9% | 214.4 | 0.1% |
| 0.18 | 247.6 | 211.0 | 14.8% | 246.6 | 0.4% |
| 0.20 | 280.0 | 238.1 | 14.9% | 278.7 | 0.5% |

Source: Elaborated by the authors.

From the Closed Vessel Testing, a pressure-time profile for six different loading densities, illustrated in Fig. 4, was obtained for formulation A, where the theoretical values calculated using PR-EoS and V2-EoS were represented in the graph as squares and circles, respectively.
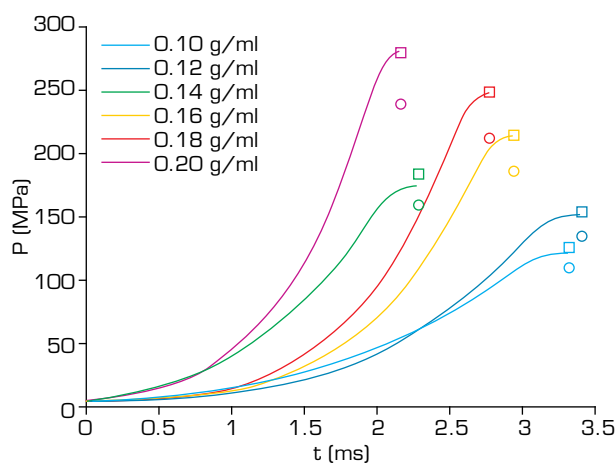


Source: Elaborated by the authors.

**Figure 4.** Experimental pressure-time profile for Formulation A for different loading densities (squares: PR-EoS; circles: V2-EoS).

The experimental load density is calculated by simply dividing the propellant mass employed by the chamber nominal volume and the experimental maximum pressure is the largest of the 3072 recorded measurements.

By analyzing the data in Table 8, it can be seen that PR-EoS gave more accurate results than V2-EoS for all the six loading densities. Moreover, except for $\Delta = 0.18$ and $0.20$ g/cm³, the remaining pressures were slightly higher than the experimental ones. On the other hand, all pressures calculated using V2-EoS were lower than the experimental values.

Considering that the main purpose of doing theoretical estimations, within the energetic materials field, is to allow empirical researchers to focus their resources on promising new energetic candidates, which offers good performance and safety, thus avoiding unnecessary costs and possible accidents. Therefore, in terms of pressure, a theoretical result that is lower than the experimental value would be undesirable, because, in the case of $\Delta = 0.16$, one might erroneously select a case material designed to support up to 200 MPa without knowing that the pressure could go up to 214.4 MPa, thus causing an accident. Therefore, for predicting maximum pressure for formulation A, PR-EoS would definitely be the better choice, since its deviations are between 0.1-5.3%.

## Calculation Results of the Adiabatic Flame Temperature and the Chemical Composition of Combustion Products

The Adiabatic Flame temperature is a thermodynamic parameter that represents the maximum temperature that combustion products can reach when this temperature was raised under adiabatic conditions as a result of the evolution of heat from the reaction itself (Munir and Anselmi-Tamburini 1989). Since this parameter reflects the energy level of propellants, its assessment contributes greatly to understand the reaction energy release process.

The theoretical approach to estimate the adiabatic flame temperature is based on the selection of a suitable PVT EoS for estimating combustion products. Since PR-EoS has proven to be more accurate than V2-EoS regarding the experimental values of maximum chamber pressure for formulation A, this paper assumed this model would also be suitable for predicting the chemical equilibrium of combustion products. Based on this assumption, both the equilibrium chemical composition of the combustion products and the adiabatic flame temperature were calculated using the PR-EoS model. Table 9 shows the predicted adiabatic flame temperature as well as the predicted molar fractions of the gases in the product of each experiment.

**Table 9.** Adiabatic flame temperature and composition of the gaseous product as functions of the load density ($\Delta$).

| $\Delta$ (g/cm³) | T (K) | $x_{CO}$ | $x_{H_2O}$ | $x_{CO_2}$ | $x_{H_2}$ | $x_{N_2}$ |
|---|---|---|---|---|---|---|
| 0.10 | 3527.8 | 0.3592 | 0.2808 | 0.1545 | 0.0689 | 0.1368 |
| 0.12 | 3528.2 | 0.3588 | 0.2798 | 0.1554 | 0.0697 | 0.1368 |
| 0.14 | 3528.5 | 0.3573 | 0.2789 | 0.1563 | 0.0707 | 0.1368 |
| 0.16 | 3528.9 | 0.3563 | 0.2779 | 0.1573 | 0.0717 | 0.1368 |
| 0.18 | 3529.3 | 0.3553 | 0.2769 | 0.1583 | 0.0726 | 0.1368 |
| 0.20 | 3529.7 | 0.3543 | 0.2759 | 0.1592 | 0.0736 | 0.1368 |

Source: Elaborated by the authors.

From Table 9 and Fig. 5, it was possible to observe how the molar fractions from the combustion products changed when the loading density increased. Since $N_2$(g) is not part of the water-gas equilibrium, its molar fraction did not suffer any change. However, for the remaining gases, it could be noticed, in Fig. 5, that whereas $x_{CO_2}$ and $x_{H_2}$ increased when the loading density increased, the opposite happened for $x_{CO}$ and $x_{H_2O}$, which means that an increase in the loading density favors the production of $CO_2$ (g) and $H_2$ (g).
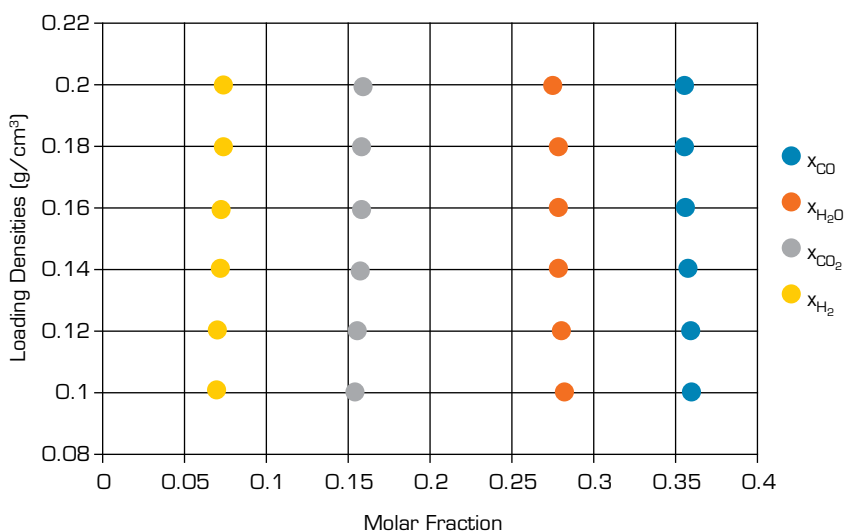
**Figure 5.** Behavior of molar fractions in function of the loading density of propellant.

By looking into data from Table 9, another correlation can be observed in Fig. 6. In this case, it was straightforward to see that the temperature increased almost linearly with the increase of the loading density of the propellant, displaying a correlation value of 0.9983. This observation is coherent, because the higher the propellant mass within the same container, the higher will be the gas production, thus leading to higher pressures and temperatures.



$$y = 18.857x + 3525.9$$
$$R^2 = 0.9983$$
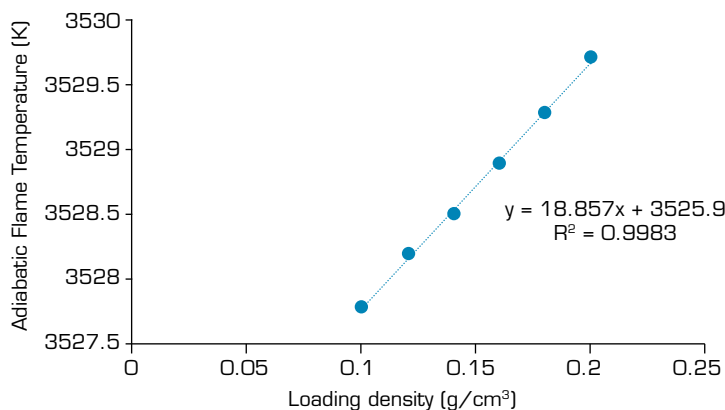
**Figure 6.** Behavior of adiabatic flame temperature in function of the loading density of propellant.

## CONCLUSION

In this paper, we investigated whether the Peng-Robinson Equation of State (PR-EoS) could predict the maximum chamber pressure of a propellant formulation more accurately than the quadratic virial equation of state (V2-EoS). To assess that, we compared the theoretical values from both models to the experimental results obtained from a ballistic closed vessel test for a propellant formulation under six different loading densities.

The comparison showed that PR-EoS could give more accurate results, since its maximum deviation was 5.3%, whereas for the V2-EoS, it was 14.9%. Besides, since all the pressures predicted by V2-EoS were lower than the measured values, this could lead to a poor selection of case material, thus resulting in an accident.

After proving that the PR-EoS was more suitable for predicting the maximum chamber pressure, this model, based on the water-gas equilibrium, was used to describe the thermodynamic state of gaseous combustion products and then the adiabatic flame temperature was calculated.

From the predicted values, we noticed that a higher loading density favors the production of $CO_2$ (g) and $H_2$ (g) and increases almost linearly the adiabatic flame temperature. Both the adiabatic flame temperature and the composition of the gaseous products are crucial to the design of tube/barrel guns or missiles/rockets that use such propellant.

## CONFLICT OF INTEREST

Nothing to declare.

## AUTHOR CONTRIBUTIONS

**Conceptualization:** Anastacio AC and Peixoto FC; **Data curation:** Silva LA, Dias ACM, Volskis HGT, Silva JDL; **Formal analysis:** Silva LA and Peixoto FC; **Acquisition of funding:** Peixoto FC; **Research:** Silva LA, Dias ACM, Volskis HGT, Silva JDL; **Methodology:** Anastacio AC and Peixoto FC; **Project administration:** Anastacio AC and Peixoto FC; **Resources:** Peixoto FC; **Software:** Peixoto FC; **Supervision:** Anastacio AC and Peixoto FC; **Validation:** Silva LA, Dias ACM, Volskis HGT, Silva JDL; **Visualization:** Silva LA and Peixoto FC; **Writing - Preparation of original draft:** Silva LA, Peixoto FC; **Writing - Proofreading and editing:** Silva LA, Dias ACM, Volskis HGT, Silva JDL, Anastacio AC, Peixoto FC.

## DATA AVAILABILITY STATEMENT

Data will be available upon request.

## FUNDING

## ACKNOWLEDGMENTS

Not applicable.

## REFERENCES

Bergan NE (1991) High-Pressure Thermodynamics in Combustion Processes (Dissertation). Davis: University of California.

Congiunti A, Bruno C (2003) Supercritical Combustion Properties. Paper presented at 41st Aerospace Sciences Meeting and Exhibit. AIAA; Reno, United States. https://doi.org/10.2514/6.2003-478

Cooper PW, Kurowski SR (1997) Introduction to the Technology of Explosives. New Jersey: Wiley.

Giorgi MG, Sciolti A, Ficarella A (2014) Application and Comparison of Different Combustion Models of High Pressure LOX/CH4 Jet Flames. Energies 7(1):477-497. https://doi.org/10.3390/en7010477

Oliveira JS, Furtado Filho AA, Platt MG, Peixoto FC (2005) Modeling of Closed-Vessel Experiments and Ballistic Parameter Estimation. J Energ Mater 23(2):59-73. https://doi.org/10.1080/07370650590936406

Dyer J, Zilliac G, Sadhwani A, Karabeyoglu A, Cantwell B (2007) Modeling Feed System Flow Physics for Self-Pressurizing Propellants. Paper presented at 43rd AIAA/ASME/SAE/ASEE Joint Propulsion Conference & Exhibit. AIAA; Cincinnati, United States. https://doi.org/10.2514/6.2007-5702

Grivell MR (1982) The Closed Vessel Test and Determination of Ballistic Properties of Gun Propellants. Adelaide: Department of Defense.

Harvazinski ME, Talley DG (2018) Evaluation of multi-phase equations of state for liquid rocket engine combustion modeling. Edwards: Air Force Research Laboratory.

Hickey J-P, Ihme M (2013) Supercritical mixing and combustion in rocket propulsion. Center for Turbulence Research Annual Research Briefs, 21-36.

Jofre L, Urzay J (2021) Transcritical diffuse-interface hydrodynamics of propellants in high-pressure combustors of chemical propulsion systems. Prog Energy Combust Sci 82:100877. https://doi.org/10.1016/j.pecs.2020.100877

Longdon LW (1987) Textbook of ballistics and gunnery. London: Her Majesty's Stationary Office.

Mallepally RR, Bamgbade BA, McHugh MA, Baled HO, Enick RM, Billingsley MC (2019) Measurements and modeling of the density of rocket propellant RP-2 at temperatures to 573 K and pressures to 100 MPa. Fuel 253:1193-1203. https://doi.org/10.1016/j.fuel.2019.05.089

Mehta P, Shetty CP, Pundkar RN, Shekhar H (2015) Effect of Loading Densities in Closed Vessel Tests on the Burning Rate of a Propelling Charge. Def Sci J 65(2):126-130. https://doi.org/10.14429/dsj.65.8158

Mukhtar A, Nasir H, Rashid B, Waheed H (2019) Development of zirconium and potassium perchlorate igniter for AP/HTPB composite propellant base bleed grain. J Therm Anal Calorim 138:3939-3947. https://doi.org/10.1007/s10973-019-08317-2

Müller H, Pfitzner M (2017) A flamelet model for transcritical LOx/GCH4 flames. J Phys: Conf Ser 821(1):012010. https://doi.org/10.1088/1742-6596/821/1/012010

Müller H, Pfitzner M, Lapenna PE, Ciottoli PP, Creta F, Valorani M (2017) Analysis of the flame structure in non-premixed methane/oxygen flames at high-pressure conditions. Paper presented at 8th European combustion meeting. Dubrovnik, Croatia.

Munir ZA, Anselmi-Tamburini U (1989) Self-propagating exothermic reactions: The synthesis of high-temperature materials by combustion. Mater Sci Rep 3(7-8):277-365. https://doi.org/10.1016/0920-2307(89)90001-7

Myint PC, McClelland MA, Nichols AL (2016) Application of the Peng–Robinson Equation of State to Energetic Materials RDX and TNT: Pure Components, Liquid Mixtures, and Solid Mixtures. Ind Eng Chem Res 55(7):2252-2266. https://doi.org/10.1021/acs.iecr.5b04808

Prausnitz JM, Poling BE, O'Connell PJ (2000) The Properties of Gases and Liquids. New York: McGraw Hill.

Rumble JR (2021) CRC Handbook of Chemistry and Physics. Boca Raton: CRC Press.

Neron L, Saurel R (2022) Noble–Abel/first-order virial equations of state for gas mixtures resulting from multiple condensed reactive materials combustion. Phys Fluids 34(1):016107. https://doi.org/10.1063/5.0079187

Smith B, Muruganandam L, Murthy L, Shantha S (2010) A Review of the Water Gas Shift Reaction Kinetics. Int J Chem React Eng 8(1):1-34. https://doi.org/10.2202/1542-6580.2238

Suceska M (1999) Calculation of thermodynamic parameters of combustion products of propellants under constant volume conditions using the virial equation of state. Influence of values of virial coefficients. J Energ Mater 17(2-3):253-278. https://doi.org/10.1080/07370659908216107

Sudarsan NV, Das SK, Naik SD (2016) Generalized Method for Gun Propellant Formulation Design. Propellants Explos Pyrotech 41(5):844-849. https://doi.org/10.1002/prep.201500316

Van Ness H, Smith JM, Abbott M, Swihart M (2017) Introduction to Chemical Engineering Thermodynamics. New York: McGraw-Hill. https://doi.org/10.1002/prep.201500316

Venugopalan S (2015) Demystifying Explosives: Concepts in High Energy Materials. Amsterdam: Elsevier. https://doi.org/10.1016/C2014-0-00328-0

Xu B, Ying S-j, Liao X (2016) Calculation of propellant gas pressure by simple extended corresponding state principle. Def Technol 12(2):86-89. https://doi.org/10.1016/j.dt.2015.12.005